J. Biomed. Eng. Res : 117-124, 2006

Implementation of an Ultrasound Elasticity Imaging System

Gae-Young Cho[1], Ra-Young Yoon[1], Jeong-Man Park[2], Sung-Jae Kwon[3],
Young-Bok Ahn[4], Moo-Ho Bae[5], Mok-Kun Jeong[6]

[1]*Research Center, Medison Daechi-dong, Gangnam-gu, Seoul*
Departments of [2]*Physics,* [3]*Communication Engineering, and* [6]*Electronic Engineering*
Daejin University Pocheon, Gyeonggi
[4]*Department of Electronic Engineering, Konkuk University Seoul*
[5]*Division of Information Engineering and Telecommunication, Hallym University*
Chuncheon, Gangweon
(Received March 22, 2006. Accepted May 25, 2006)

Abstract

Recently, active research has been going on to measure the elastic modulus of human soft tissue with medical ultrasound imaging systems for the purpose of diagnosing cancers or tumors which have been difficult to detect with conventional B-mode imaging techniques. In this paper, a real-time ultrasonic elasticity imaging system is implemented in software on a Pentium processor-based ultrasonic diagnostic imaging system. Soft tissue is subjected to external vibration, and the resulting tissue displacements change the phase of received echoes, which is in turn used to estimate tissue elasticity. It was confirmed from experiment with a phantom that the implemented elasticity imaging system could differentiate between soft and hard regions, where the latter is twice harder than the former, while operating at an adequate frame rate of 20 frames/s.

Key words : complex baseband, displacement estimation, elasticity imaging, ultrasound, vibration

Ⅰ. INTRODUCTION

In medical ultrasonic imaging systems, the B-mode imaging modality utilizes the difference in acoustic impedance to image echo signal magnitude, but suffers from the poor capability of detecting lesions such as cancers or tumors in soft tissues, because the boundaries between lesions and normal tissues are not clearly delineated. There have been various efforts to characterize tissue parameters, e.g., attenuation coefficient, speed of sound, and nonlinear parameter [1,2], but it was difficult to obtain satisfactory results due to complicated interaction between ultrasound and human tissue. Among imaging modalities that can image or measure tissue properties, ultrasonic elastography is attracting much attention from the research community because it is based on the observation that tissue elasticity varies greatly between normal and cancerous tissues, and thus is relatively amenable to measurement.

Corresponding Author : Mok-Kun Jeong
Department of Electronic Engineering, Daejin University, Pocheon, Gyeonggi, 487-711
Tel : 031-539-1904 / HP : 011-752-1904
E-mail : jmk@daejin.ac.kr

Elastography (i.e., elasticity imaging) measures the amount of tissue displacement resulting from the application of compression to human tissue, and presents it in the form of an image. If cancerous tissue enclosed by normal tissue inside a human body is subjected to externally applied compression, the former deforms less than the latter because there is a difference in their respective elastic properties. Measurement of the deformation or displacement can lead to the estimation of tissue stiffness which is not available with the current B-mode imaging technique, enabling the possible diagnosis of cancer. In recent years, efforts have been underway to develop real-time elastographic scanners. Now they are matured to be in the stage of clinical evaluation for purposes of detecting breast and prostate cancers.

Elastographic imaging methods can be categorized depending on how stress is applied to human tissue. In one method, compression is applied externally to a tissue of interest, and the amount of tissue shift between pre- and postcompression echoes is computed using their crosscorrelation function. This new method was introduced and termed elastography by Ophir et al. [3]. Yamakoshi et al. [4] proposed a method of imaging mechanical vibration characteristics of human tissue

subjected to external vibration, presenting the amplitude and phase maps of internal vibrations in tissue undergoing forced low-frequency vibration. Gao et al. [5] further analyzed it theoretically, and presented images of tissue vibration obtained by using the Doppler method. Also, Park et al. [6] derived wave equations governing wave propagation in media for various vibration frequencies and medium characteristics, and discussed the potential of sonoelastography for lesion detection. Ahn et al. [7] estimated tissue elasticity by capitalizing on the temporal variation of ultrasonic image brightness variance in response to externally applied vibration.

In this paper, in order to obtain elasticity images in real time, we implement a system for imaging the vibration characteristics of a medium of interest by subjecting it to mechanical vibration. Although our previous implementation works involved the use of freehand compression, the system was experimental, and the results were preliminary [8,9], the present paper presents the details of full implementation of real-time strain imaging using externally applied vibration.

In this paper, we have implemented an elastographic imaging system by indirectly measuring the temporal change in phase of return echoes using demodulated complex baseband signals. To this end, we have constructed circuits to obtain demodulated signals from a diagnostic ultrasound scanner, and used the acquired data to produce elasticity images in real time on a PC platform that the scanner is based on.

II. METHODS

A. Elasticity Imaging Theory

If we apply mechanical vibration to a human body, the vibration amplitude therein varies depending on the tissue characteristics. This behavior is due to the difference in hardness between constituent tissue cells, and the vibration amplitude is inversely proportional to their elastic moduli [6,10]. Therefore, the measurement of vibration amplitude leads one to estimate the elastic modulus of tissue. When mechanical vibration whose frequency ranges from 50 to 500 Hz is applied outside of the human body, soft tissues inside the body exhibit different vibration amplitudes depending on their stiffness values. The higher the vibration frequency, the more difficult it is to penetrate deeply into the body. Hence, in general, vibration frequencies around 100 Hz are used. However, as the vibration frequency decreases, the resolution of elasticity image tends to decrease. Accordingly, we need to vary the frequency and amplitude of vibration appropriately such that we may obtain good elasticity image quality. Vibrational elasticity imaging produces elasticity images from vibration patterns around a vibration source. Placing the vibration source deep into the body makes it possible to obtain an elasticity image of the inside human body.

The Doppler method can be employed in estimating the vibration amplitude of tissue, but it suffers from reduced data acquisition rate and complex hardware [5]. To overcome the limitations of the Doppler method, in this paper we measured phase change with time at individual pixels using the same RF data acquired to produce B-mode images [8,11-14]. The same scanlines in two consecutive frames that are temporally adjacent have little phase difference in the absence of externally applied vibration, but when there is vibration, the phase difference will appear. Recognizing that the phase change is proportional to the vibration amplitude of tissue, we can measure tissue stiffness indirectly without additional hardware.

The difference in phase between the same scanlines in two consecutive frames is computed by assuming that they are of the same waveform and there is a time delay that can be represented as a linear phase, i.e., flat group delay between them. Since, however, the bandwidth of ultrasonic signals is typically large, we reduced the accompanying phase estimation errors by compensating for the center frequency shift with increasing propagation depth [11].

The strain measurement method of estimating displacement from phase change processes the inphase (I) and quadrature (Q) components of a complex baseband signal demodulated from RF. The motion displacement of the same scanlines from the previous to the present frame is computed, and then the strain is obtained as the differentiation of the estimated displacement [9]. Demodulated complex data are normalized. Only the magnitude part of the data is processed so that the phase part remains unchanged. This normalization step helps reduce impulsive noise.

$$I_n(i,j) = I(i,j)/[\sqrt{I^2(i,j)+Q^2(i,j)}+\alpha]$$
$$Q_n(i,j) = Q(i,j)/[\sqrt{I^2(i,j)+Q^2(i,j)}+\alpha] \quad (1)$$

where the ith axial point and the jth scanline together indicate each pixel position, $I(i,j)$ and $Q(i,j)$ denote, respectively, the inphase and quadrature components before normalization, $I_n(i,j)$ and $Q_n(i,j)$ denote both components, after normalization, and α is a normalization constant. The effect of normalization becomes more pronounced as we increase the value of α. Suitable values of α were empirically found to be in the range of 0.1 to 10. In simulation studies, we obtained good results when α was set to 0.5.

To estimate tissue displacement, the phase difference and instantaneous frequency are estimated by carrying out 1-D

correlation operation on the normalized inphase and quadrature components. Letting $x_{b1}(i,j)$ and $x_{b2}(i,j)$ denote the complex baseband signals whose real part is $I_n(i,j)$ and imaginary part is $Q_n(i,j)$ in the current and previous frames, respectively, we obtain the phase difference between frames, $\Delta\Phi(i,j)$, and the instantaneous frequency, $\phi'(i,j)$, as follows:

$$\Delta\Phi(i,j) = \sum_{i=-L/2}^{L/2} x_{b1}(i,j) \cdot x_{b2}^{*}(i,j) \tag{2}$$

$$\phi'(i,j) = w_B(i,j) = \frac{1}{T} \sum_{i=-L/2}^{L/2} x_{b1}(i+1,j) \cdot x_{b1}^{*}(i,j) \tag{3}$$

where L is the size of a window used to compute correlation. The instantaneous frequency accounts for the center frequency shift due to attenuation. From both (2) and (3), denoting the center frequency in rad/s by w_0, we get the displacement $\tau(i,j)$ as follows:

$$\tau(i,j) = \frac{\Delta\Phi(i,j)}{w_o + w_B(i,j)} \tag{4}$$

Dividing both sides of (4) by the sampling interval T in the axial direction, we get the normalized time delay $\tau_n(i,j)$ as:

$$\tau_n(i,j) = \frac{\tau(i,j)}{T} = \frac{\Delta\Phi(i,j)}{T[w_o + w_B(i,j)]} \tag{5}$$

Due to aliasing, the normalized time delay obtained is bounded by the range $|\tau_n| < 0.5$. Since the differentiation operation produces a large value at the point where aliasing occurs, we compensate for the estimated time delay. This process is referred to as phase unwrapping, and is given by (6). Letting $X(i,j) = \tau_n(i,j) - \tau_n(i+1,j)$, we check to see if $X(i,j)$ is less than or greater than 0.5. If it is less than 0.5, we increment it by 1; otherwise, we decrement it by 1. Mathematically, the process of obtaining the unwrapped $X_{unwrap}(i,j)$ can be described as follows:

$$X_{unwrap}(i,j) = \begin{cases} X(i,j)+1, X(i,j) < 0.5 \\ X(i,j)-1, X(i,j) > 0.5 \end{cases} \tag{6}$$

If we differentiate the temporal phase change with respect to depth, we obtain elasticity images. To improve image quality, we apply postprocessing, including median filtering, spatial average filter, logarithmic compression, and persistence control. In postprocessing, the median and spatial average filters serve to reduce intraframe noise. Persistence control suppresses image noise in the temporal direction using the following expression:

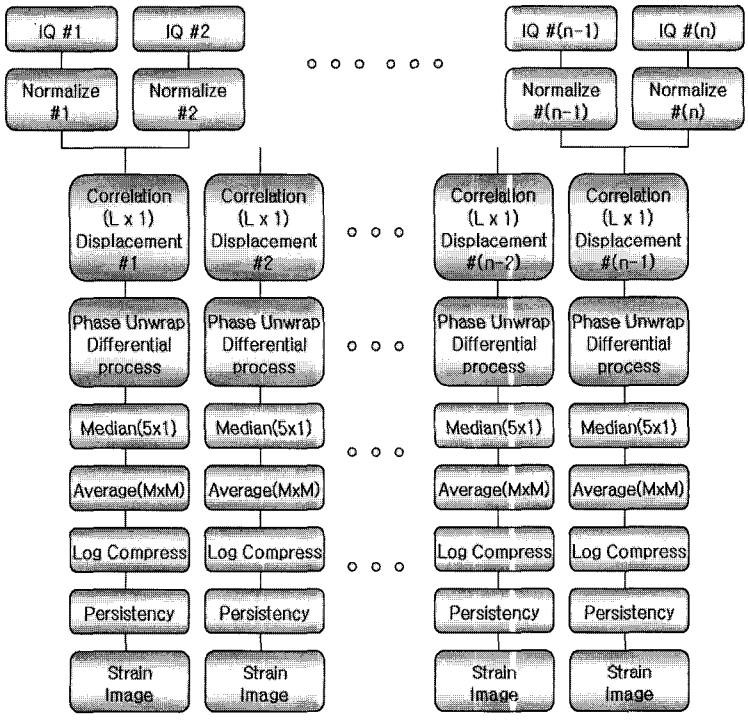

Fig. 1. Overall signal processing flow where L is the correlation window length and M is the average filter size.

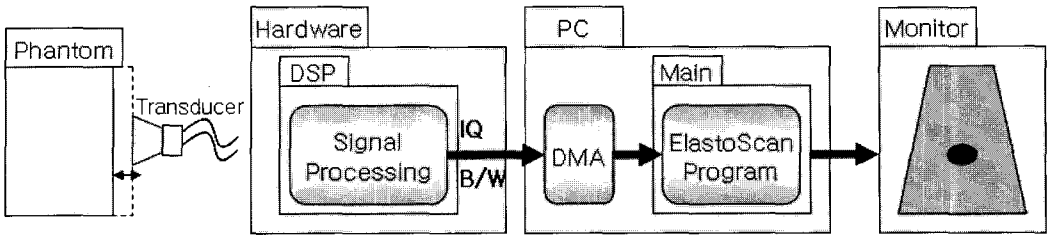

Fig. 2. Configuration of elasticity imaging system

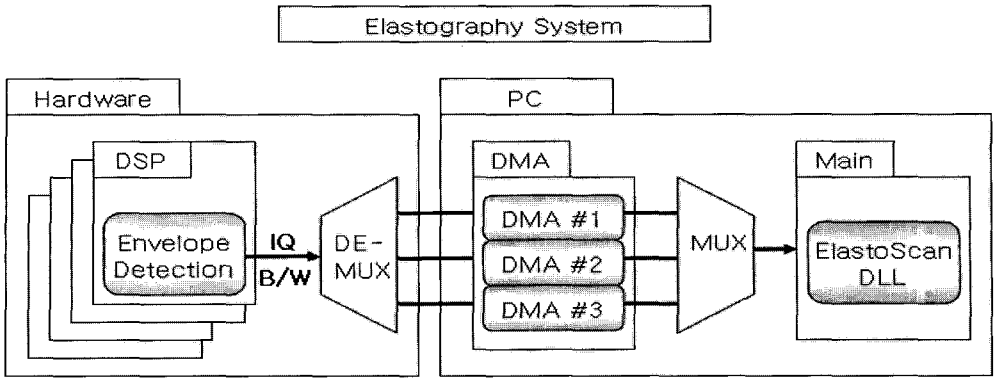

Fig. 3. Configuration of elasticity imaging system: details of data transfer.

$$S_k(i,j) = pS_{k-1}(i,j) + (1-p)X_k(i,j) \quad (7)$$

where the (i,j) index indicates the pixel position, $X_k(i,j)$ is the current input data, $S_k(i,j)$ is the current output data, and $S_{k-1}(i,j)$ is the previous output data. Following all the above postprocessing, we obtain elasticity images. The above elasticity estimation process consists of nine steps shown in Fig. 1, and we can set relevant parameters in each step.

B. Elasticity Imaging System

Real-time elasticity imaging was implemented on a diagnostic ultrasound scanner (ACCUVIX XQ, Medison, Seoul, Korea) [15]. The scanner is built around a PC with a 2 GHz Pentium 4 microprocessor and 1 GB of memory. The system operates under the Windows NT operating system. The implemented real-time elasticity imaging system built on the ultrasound scanner can be divided into hardware and software parts. We proceed to explain their respective roles. The hardware part is responsible for signal processing tasks relating to ultrasound B-mode imaging, where both B/W and I/Q data are computed. Here, the B/W data refer to the detected B-mode image data. Both B/W and I/Q data obtained in this way are transferred to the PC platform using direct memory access (DMA), and are processed in software on a

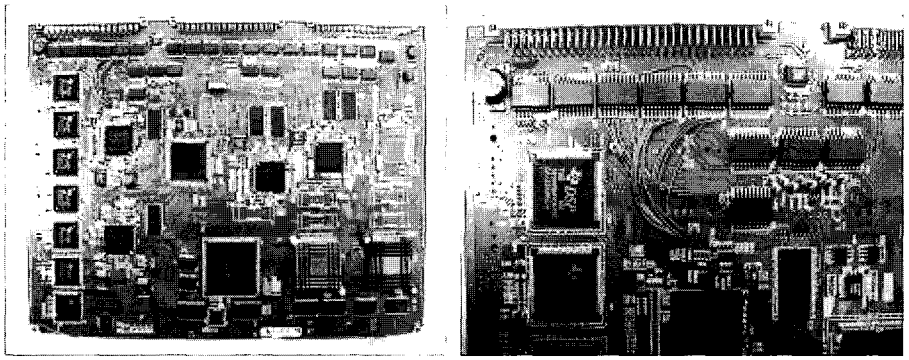

Fig. 4. The left panel shows the modified DSP board, and the right panel is an enlarged view of the modified area.

real-time basis to estimate elasticity. The results are converted into elasticity images and displayed on a monitor.

Fig. 2 shows the configuration of our elasticity imaging system. The ultrasound scanner on which the elasticity imaging system is built provides data required for elasticity computation, and the elasticity estimation algorithm is implemented in software, but not in hardware. This design methodology facilitates implementation and modification. The elasticity estimation algorithm is written as a Visual C++ dynamic link library (DLL), and is called by the main program which takes care of the graphical user interface (GUI) of the ultrasound scanner.

More specifically, in the hardware part, a DSP board is devoted to all signal processing tasks. As soon as a whole frame of detected B-mode brightness data, i.e., B/W data, and complex I/Q data are processed, they are transferred to the PC and stored in the DMA memory. The demultiplexer in Fig. 3 sequentially selects one of the three DMA memories. The use of three DMA memories are intended to prevent data from being overwritten before being read out. The data stored in the DMA memories are read out sequentially to the multiplexer shown in Fig. 3. The main program calls the DLL routine for the elasticity estimation procedure, referred to in Figs. 2 and 3 as "ElastoScan," which in turn processes the read data to provide elasticity images in real time.

Most of the signal processing required for ultrasonic image formation is accomplished in a DSP board inside the ultrasound scanner. The DSP board processes the RF data coming from the beamformer to produce B/W data, which constitute the fundamental B-mode image, as well as I/Q data. The I/Q data are processed further to obtain and display color Doppler information as well. The DSP board already available in the ultrasound scanner could process B/W data, but did not have provisions for processing the I/Q data. So we have modified it. The right panel of Fig. 4 shows the modified DSP board to make the I/Q data available for subsequent processing to produce elasticity images. Jumpers shown on the PCB in Fig. 4 are the data and control buses.

The I and Q data bus consists of 16 bits, and plays the role of transferring data through DMA. One frame of ultrasonic image data consists of one frame of I and Q data each. The I and Q data processed in the DSP board are stored in the DMA memories in order of one frame of I followed by one frame of Q data. So the I and Q data amount in total to two frames of B-mode image data. Thus, the elasticity estimation program needs to keep track of the I and Q data to separate them according to the order of having stored them. The B/W data have a data width of eight bits, and one frame of B-mode image has the same amount of B/W data. Hence, there is no need to separate the B/W data in the program, unlike the case of the I and Q data.

III. MATERIALS

We fabricated a phantom and vibrator to verify the performance of the developed real-time elasticity imaging system built around a diagnostic ultrasound scanner. The phantom was fabricated by mixing an agar and gelatin sample with carbon powder, propane, alcohol, formalin, or glutaraldehyde, and then letting it cool down in room temperature. We adjusted the amount of gelatin in the sample to control its hardness [16].

The material composition of two phantoms A and B fabricated in house is presented in Table 1. Phantom A which is harder than phantom B is used as a cylindrical inclusion, while the latter is used as the surrounding background. The whole phantom is of size 12 cm × 16 cm × 12 cm, where the cylindrical inclusion located at a depth of 2.8 cm is harder than the background by a factor of two. The factor of two was selected because it represents the typical ratio of the elastic moduli of abnormal (100 kPa) to normal (62 kPa) tissues of a human prostate [17], and also because it is a small enough elasticity contrast allowing us to test the system's ability to detect lesions with small differences in elastic modulus. For example, the average shear modulus of fibroadenoma is about four times harder than normal breast tissue, and carcinomas are about eight times harder than fibroadenomas [17]. Fig. 5 is a perspective view of the fabricated elasticity phantom.

The left and right panels of Fig. 6 are, respectively, a photograph of the diagnostic ultrasound scanner and the experimental setup. The elasticity imaging system presented in the present paper requires the use of a vibrator, the choice of which has a significant effect on elasticity image quality.

Table 1. Specifications of fabricated phantoms A and B (x means no addition).

Phantom	Agar (g)	Gelatin (g)	Carbon (g)	Alcohol (cc)	Formalin (cc)	Glutar-aldehyde (cc)	Water (cc)
A	18	216	10	140	x	18	1398
B	18	180	10	140	18	x	1434

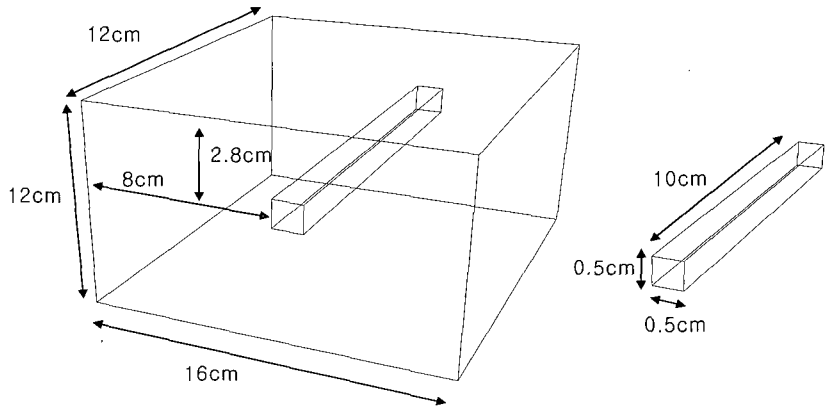

Fig. 5. A 3-D view of the fabricated phantom.

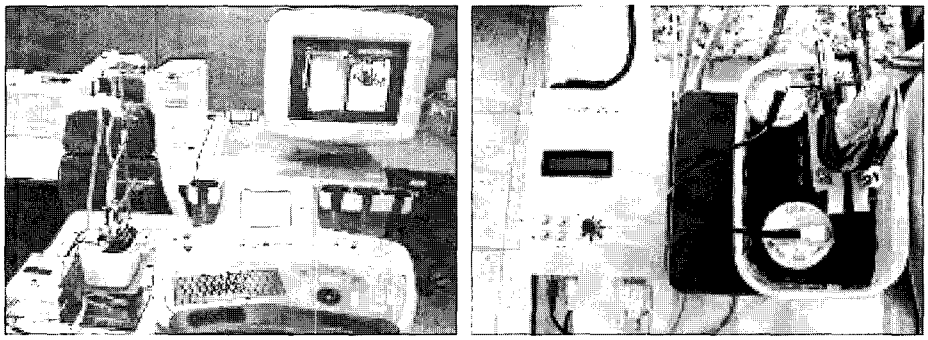

Fig. 6. The left panel shows the ultrasound scanner, and the right panel shows the in-house made signal generator, vibrator, and phantom.

Brüel & Kjær [18] manufactures and markets modal exciters, vibration exciters, and mini-shakers, among which a mini-shaker was used by the Fink group in their experiments [19]. However, those vibrators tend to be bulky and heavy, thereby being unsuitable for diagnostic imaging purposes. This necessitated the in-house construction of a new vibrator whose vibration frequency meets the range between 20 Hz and 500 Hz and whose vibration amplitude is greater than 1 mm when driven by a continuous wave of 2 to 3 W. It is desirable that the new vibrator could be easily coupled to a transducer, or should make a good contact with the human body, preferably in the form of a detachable patch.

Ⅳ. RESULTS

Fig. 7 displays a popup menu where relevant imaging parameters can be set by the user for optimum results. The menu is implemented in the developed elasticity imaging system. Those parameters can be set as we wish during experimentation. To achieve optimum elasticity image quality, besides setting parameters available in the popup menu, we adjusted the vibration frequency as well as the vibrator position. Data were acquired for both cases of mechanically fixing the transducer to a support and holding it in hand. The latter configuration is important in assessing the effect of hand motion on elasticity estimation.

The first experiment in which the transducer was fixed to be unmovable was designed to obtain elasticity images due only to the vibration excluding the effect of all other movements. In the second experiment, the transducer was held in hand, and elasticity images were produced while vibration was applied externally. The hand movement or the transducer position change acts as a source of large noise, like externally applied vibration.

We can find out the effect of extraneous noise on elasticity estimation from these two experiments. The vibration frequency was set to 120 Hz, and the whole phantom described above was used in experiment. The right two panels of Figs. 8 and 9 are the elasticity images obtained by fixing the transducer and by holding the transducer in hand, respectively, while the left two panels correspond to the B-mode images. For the case of holding the transducer in hand, the inclusion representative of a tumor looks somewhat larger than its actual size.

Nevertheless, it can be seen from Figs. 8 and 9 that the stiffer inclusions can be differentiated from the normal background. However, this is not the case for the B-mode

images, as can be seen in the left two panels of Figs. 8 and 9.

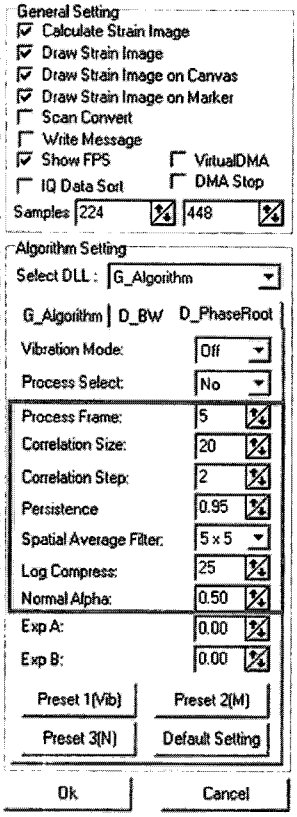

Fig. 7. Popup menu for parameter setting in ultrasound scanner.

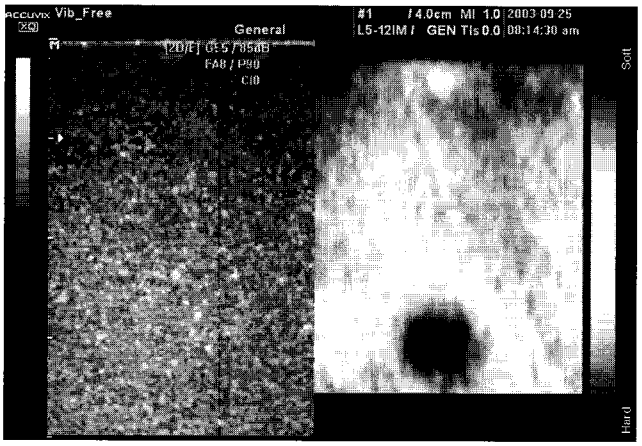

Fig. 8. B-mode image (left) and elasticity image (right) obtained while fixing the transducer mechanically.

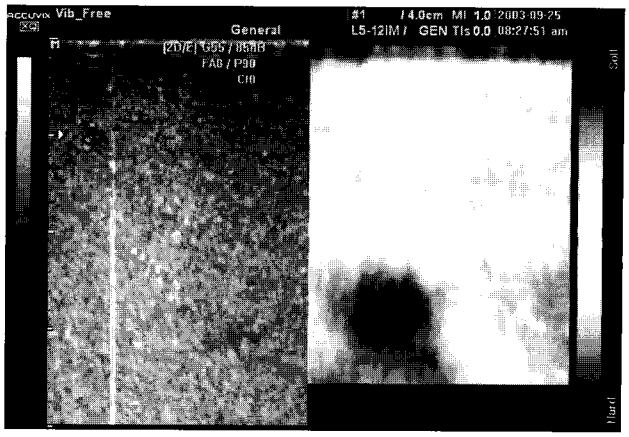

Fig. 9. B-mode image (left) and elasticity image (right) obtained while holding the transducer in hand.

V. CONCLUSION

In this paper, we have implemented a real-time elasticity imaging system using a method of estimating tissue displacements from phase differences representing the mechanical vibrational amplitude of soft tissue subjected to externally applied vibration. It is built on top of a commercial diagnostic ultrasound scanner (ACCUVIX XQ, Medison, Seoul, Korea). Both B/W and I/Q data processed in the hardware board are stored in DMA memory units, and the elasticity estimation algorithm implemented in software produces elasticity images for display on a monitor at a rate of 20 frames/s.

To verify the performance of the elasticity imaging system, we fabricated an agar-gelatin phantom where a 5 mm diameter cylindrical inclusion is embedded in the background medium and the former was made to be two times harder than the surrounding background. We experimented with two types of applying vibration to the phantom: one is mechanically fixing the transducer, and the other is holding the transducer in hand. Both methods produced comparable elasticity images. We confirmed by experiment the efficacy of the implemented elasticity imaging system. Artifacts and noise need to be further reduced for application in real world clinical environments.

Up to now, we have elaborated on the implementation of a real-time elasticity imaging system and its performance. To make the real-time elasticity imaging system a useful diagnostic imaging tool in the near future, we need to focus efforts to reduce the computational complexity as well as to enhance the accuracy of estimating tissue elasticity, and to come up with an easy and reproducible method of measuring it. These two aspects need to be further investigated in much

more detail. It is expected that the elasticity imaging system developed here will find its way to clinical use through further performance optimization and clinical evaluations.

REFERENCES

[1] P. A. Lewin, "Diagnostic imaging of the nonlinear acoustic parameter B/A," *J. Acoust. Soc. Amer.*, vol. 79, pp. S44-S45, 1986.

[2] C. A. Cain, H. Nishiyama, and K. Katakura, "On ultrasonic techniques for measurement of the nonlinear parameter B/A in fluid-like media," in *Proc. IEEE Ultrason. Symp.*, 1986, pp. 885-888.

[3] J. Ophir, I. Cespedes, H. Ponnekanti, Y. Yazdi, and X. Li, "Elastography: A quantitative method for imaging the elasticity of biological tissues," *Ultrason. Imag.*, vol. 13, pp. 111-134, 1991.

[4] Y. Yamakoshi, J. Sato, and T. Sato, "Ultrasonic imaging of internal vibration of soft tissue under forced vibration," *IEEE Trans. Ultrason. Ferroelect. Freq. Contr.*, vol. 37, pp. 45-53, 1990.

[5] L. Gao, S. K. Alam, and K. J. Parker, "A new vibration theory for sonoelasticity imaging", in *Proc. IEEE Ultrason. Symp.*, vol. 2, 1993, pp. 879-882.

[6] J. M. Park, S. J. Kwon, and M. K. Jeong, "Wave generation and its effect on lesion detection in sonoelastography: Theory and simulation study," *J. Acoust. Soc. Korea*, vol. 25, pp. 282-293, 2005.

[7] D. K. Ahn, J. M. Park, S. J. Kwon, and M. K. Jeong, "A study on the stiffness estimation in soft tissue using speckle brightness variance tracking", *J. Biomed. Eng. Res.*, vol. 24, pp. 141-149, 2003.

[8] M. K. Jeong, J. M. Park, S. J. Kwon, and G. Y. Cho, "Realization of realtime tissue stiffness estimation in medical ultrasound imaging system," in *Proc. Int'l Conf. Ultrason. Meas. Imag. Tissue Elasticity, Corpus Christi*, Texas, USA, 2003.

[9] R. Y. Yoon, S. J. Kwon, M. H. Bae, and M. K. Jeong, "Implementation of strain imaging modality in medical ultrasonic imaging system," *J. IEEK*, vol. 42, pp. 53-62, 2005.

[10] M. K. Jeong and S. J. Kwon, "Tissue stiffness imaging method using temporal variation of ultrasound speckle pattern," *IEEE Trans. Ultrason. Ferroelect. Freq. Contr.*, vol. 50, pp.457-460, 2003.

[11] M. K. Jeong, J. M. Park, and S. J. Kwon, "Tissue stiffness measurement using vibrational force in medical ultrasound imaging system," in *Proc. Inter-Noise*, Jeju, Korea, 2003.

[12] Y. B. Ahn, M. K. Jeong, S. J. Kwon, and M. J. Choi, "Imaging of thermally ablated tissue using ultrasonic elastography," *Key Engineering Materials,* vol. 272, pp. 2042-2047, 2004.

[13] J. M. Park, S. J. Kwon, and M. K. Jeong, "A study of vibration characteristics for ultrasonic elasticity imaging," in *Proc. Int'l Conf. Ultrason. Meas. Imag. Tissue Elasticity*, Lake Windermere, United Kingdom, 2004.

[14] J. M. Park, S. J. Kwon, M. K. Jeong, and M. H. Bae, "Theoretical and simulation study of wave generation and its effect on lesion detection in sonoelastography," in *Proc. Int'l Conf. Ultrason. Meas. Imag. Tissue Elasticity*, Austin, Texas, USA, 2005.

[15] Medison, http://www.medison.com and http://www.accuvix.com.

[16] T. J. Hall, M. F. Insana, and T. A. Krouskop, "Phantom materials for elastography," *IEEE Trans. Ultrason. Ferroelect. Freq. Contr.*, vol. 44, pp. 1355-1365, 1997.

[17] T. A. Krouskop, T. M. Wheeler, F. Kallel, B. S. Garra, and T. Hall, "Elastic moduli of breast and prostate tissues under compression," *Ultrason. Imag.*, vol. 20, pp. 260-274, 1998.

[18] Brüel and Kjær, http://www.bksv.com and http://www.bksv.co.kr.

[19] M. Fink, L. Sandrin, M. Tanter, S. Catheline, S. Chaffai, J. Bercoff, and J. L. Gennisson, "Ultra high speed imaging of elasticity," in *Proc. Ultrason. Symp.*, 2002, pp. 1811-1820.